

Article

Power Generation in Slope-Type Thin-Film Thermoelectric Generators by the Simple Contact of a Heat Source

Hiroki Yamamuro and Masayuki Takashiri * 

Department of Materials Science, Tokai University, 4-1-1 Kitakaname, Hiratsuka, Kanagawa 259-1292, Japan; 7bajm043@mail.u-tokai.ac.jp

* Correspondence: takashiri@tokai-u.jp; Tel.: +81-463-58-1211

Received: 30 November 2018; Accepted: 21 January 2019; Published: 22 January 2019



Abstract: To conveniently generate electric energy for next-generation smart network monitoring systems, we propose the design and fabrication of slope-type thin-film thermoelectric generators by the simple contact of a heat source. N-type Bi_2Te_3 films and p-type Sb_2Te_3 films were formed on a stainless-steel substrate employing potentiostatic electrodeposition using a nitric acid-based bath, followed by a transfer process. In order to naturally induce a temperature difference (ΔT) between the ends of the generator, slope blocks made by polydimethylsiloxane (PDMS) were prepared and then inserted between the generators and heat sources. The performance of the generators, the open circuit voltage (V_{oc}), and the maximum output power (P_{max}), were measured using PDMS slope angles as the temperature of the heat source was increased. The ΔT of the generators increased as the slope angle was increased. The generator with the highest slope angle (28°) exhibited a V_{oc} of 7.2 mV and P_{max} of 18.3 nW at ΔT of 15 K for a heat source temperature of 42°C . Our results demonstrate the feasibility of slope-type thin-film thermoelectric generators, which can be fabricated with a low manufacturing cost.

Keywords: electrodeposition; transfer process; slope block; thin films; thermoelectric generators

1. Introduction

Thermoelectric power generators are solid-state devices that can directly convert a temperature gradient into electric power. As there are no moving parts or liquid/gas medium, they have the potential to be highly reliable and environmentally friendly energy conversion systems. The thermoelectric generators consist of p- and n-type semiconducting pillars connected by metal electrodes. In addition, there are two types of thermoelectric generators, the bulk type and the thin-film type. Conventionally, thermoelectric generators of the bulk type have been used in places with relatively high-temperature heat sources, including waste heat from automobile engines and incinerators [1–3]. However, as the Internet of things (IoT) is currently generating a great deal of interest in relation to next-generation smart network monitoring systems, thermoelectric generators using low-temperature heat sources are increasingly important [4]. In IoT technology, autonomous sensors are expected to play an important role in a wide spectrum of applications, including medical monitoring, emergency response, and industrial and environment controls [5]. These autonomous sensors need to perform functionally independent operations without changing batteries and requiring additional maintenance. Thermoelectric generators satisfy the requirements of autonomous sensors. They can semi-permanently generate electric power from various places with low-temperature heat sources, such as human bodies and hot water pipes, due to their flexibility [6,7].

Compared with their bulk counterparts, thin-film thermoelectric power generators are more likely to be suitable for powering autonomous sensors, since they are lightweight, and can be miniaturized

to generator size and processed with a lower manufacturing cost. To date, there have been many studies on thin-film thermoelectric generator fabrication using various film deposition methods, including evaporation [8–10], sputtering [11–13], and electrodeposition [14–16]. In addition, thin film thermoelectric materials possess favorable features that are not exhibited by bulk materials. The presence of nanostructured materials, including superlattices [17–19] nanocrystals [20–22], nanoporous structures [23–25], and inducing stresses [26–28], enhances the thermoelectric performance. The thermoelectric performance is defined as the figure of merit, $ZT = S^2 \sigma T / \kappa$, where S is the Seebeck coefficient, σ is electrical conductivity, and κ is thermal conductivity. Since thin-film thermoelectric materials are affected by the thermal conductivity of the substrate, their performance is mainly determined by the electrical part indicated by the power factor, $P.F. = S^2 \sigma$.

However, thin-film thermoelectric generators struggle to generate a temperature difference in the cross-plane direction. Since thin-film thermoelectric generators have relatively long pillar shaped structures, it is possible to generate the temperature difference in the in-plane direction [29–33]. For instance, Jacquot et al. [34] invented on-membrane thermoelectric generators and optimized the geometry of generators using model calculations. Takayama et al. [35] fabricated multi-layered-stack thermoelectric generators and exhibited electric power by applying a temperature difference in the in-plane direction. When the design of thin-film thermoelectric generators is optimized, they can generate electric power by adding a heat source without applying an arbitrary temperature difference between the hot and cold sides.

In this study, thin-film thermoelectric generators were fabricated using electrodeposition and transfer processes. This combined approach both takes advantage of electrodeposition and compensates for its disadvantages [36]. We used bismuth telluride (Bi_2Te_3) and antimony telluride (Sb_2Te_3) as the n- and p-type thermoelectric materials, respectively, because these materials exhibit a high figure of merit near room temperature (RT) [37,38]. In order to effectively generate a temperature difference in the generators, a slope-shaped material with low-thermal conductance was attached to the back of the generator. We changed the angle of the slope blocks and measured temperatures both proximal and distal to the heat source. The performance of the generators, the open circuit voltage (V_{oc}), and maximum output power (P_{max}), were measured by changing the temperature of the heat source.

2. Experimental Approach

Prior to the fabrication of slope-type thin-film thermoelectric generators, we prepared n-type Bi_2Te_3 and p-type Sb_2Te_3 thin films using potentiostatic electrodeposition and a standard three-electrode cell; we then measured their thermoelectric properties. The basic setup used for the electrodeposition of both thin films has been described in our previous reports [14,39,40]. A stainless-steel substrate with a thickness of 80 μm was used as the working electrode (electrode area: 1.5 cm^2), and a platinum-coated titanium mesh on a titanium plate was used as the counter electrode (combined area electrode of the mesh and plate: 1.5 cm^2). An Ag/AgCl (saturated KCl) electrode was used as the reference electrode. A potentiostat/galvanostat (Hokuto Denko, Osaka, Japan, HA-151B) was used to control the voltage at -0.01 V vs. Ag/AgCl standard electrode. For fabricating the Bi_2Te_3 thin films, nitric acid (0.4 M; diluted with deionized water) containing 2.0 mM $\text{Bi}(\text{NO}_3)_3$ (99.9%) and 3.0 mM TeO_2 (99.9%) was used as the electrolyte solution; the initial pH was approximately 1.0. For preparing the Sb_2Te_3 thin films, nitric acid (0.4 M; diluted with deionized water) containing 0.83 mM SbF_3 (99.9%) and 1.3 mM TeO_2 (99.9%) was used as the electrolyte solution; the initial pH was approximately 1.0. The thickness of both types of the thin films was approximately 1 μm .

Following electrodeposition, thermal annealing was performed to improve the thermoelectric properties of the thin films. The basic annealing procedure is described in our previous report [41]. In brief, the furnace was filled with a mixture of argon (95%) and hydrogen (5%) gases at atmospheric pressure. The gas flow rate was maintained at 1.0 L/min throughout the annealing process. The annealing condition was 250 $^\circ\text{C}$ for 1 h. Following the thermal annealing, the samples were left to cool to below 50 $^\circ\text{C}$ in the furnace.

After thermal annealing, to avoid complications arising from electrical conduction through the stainless-steel substrate, the film was fixed on a glass plate using epoxy resin, and the thin film was subsequently removed from the stainless-steel substrate. The in-plane Seebeck coefficient, S , of the thin films was measured near RT with an accuracy of $\pm 10\%$. The Seebeck coefficient was measured by connecting one side of the film to a heater and the other side to a heat sink kept near RT, with a temperature difference of <4 K between both the sides. The sheet resistance, R_s , was measured near RT using the four-point probe method (RT-70V, NAPSON, Tokyo, Japan), and the in-plane electrical conductivity, σ , was estimated from the sheet resistance and the film thickness. Both the Seebeck coefficient and sheet resistance were measured thrice at different portions of each sample to extract the average values. Finally, the in-plane power factor, $S^2 \sigma$, was estimated from the measured Seebeck coefficient and electrical conductivity. The fabrication process of the slope-type thin-film thermoelectric generators is described in Section 3.2. The measuring method for the performance of the slope-type thin-film thermoelectric generators is described in Section 3.3.

3. Results and Discussion

3.1. Thermoelectric Properties of n-Type Bi_2Te_3 and p-Type Sb_2Te_3 Thin Films

Table 1 presents the in-plane thermoelectric properties, Seebeck coefficient, sheet resistance, and estimated power factor, of the thin films. The n-type Bi_2Te_3 thin film exhibited a Seebeck coefficient of $-80 \mu\text{V}/\text{K}$, sheet resistance of $6.0 \Omega/\text{square}$ and estimated power factor of $5.2 \mu\text{W}\cdot\text{cm}^{-1}\cdot\text{K}^{-2}$. On the other hand, the p-type Sb_2Te_3 thin film exhibited a Seebeck coefficient of $100 \mu\text{V}/\text{K}$, sheet resistance of $12 \Omega/\text{square}$, and estimated power factor of $8.8 \mu\text{W}\cdot\text{cm}^{-1}\cdot\text{K}^{-2}$. The thermoelectric properties of both types of thin films were significantly higher than those of corresponding thin films in our previous study, because the thin films in this study were thermally annealed [36]. In addition, the thin films in this study exhibited comparable values when compared to well-established thin films prepared using electrodeposition [42]. After fabricating the thin-film generators, we calculated the electrical resistance of the generators based on the thermoelectric properties of the n- and p-type thin films.

Table 1. Thermoelectric properties of the n- and p-type thin films fabricated by electrodeposition.

Properties	S ($\mu\text{V}/\text{K}$)	R_s (Ω/square)	Estimated P.F. ($\mu\text{W}\cdot\text{cm}^{-1}\cdot\text{K}^{-2}$)
n-type film	-80	6.0	5.2
p-type film	100	12.0	8.8

3.2. Fabrication of Slope-Type Thin-Film Thermoelectric Generators

After determining the electrodeposition conditions of n-type Bi_2Te_3 and p-type Sb_2Te_3 thin films, we fabricated the slope-type thin-film thermoelectric generators. Figure 1 shows a schematic flow diagram of the process employed. Fabrication of the thin-film thermoelectric generators consists of two steps, fabrication of the thin-film thermoelectric generator and of the polydimethylsiloxane (PDMS) slope blocks. We used PDMS for the slope blocks, because it has both flexibility and a relatively low thermal conductivity [43].

For fabricating the thin-film thermoelectric generator (left side in Figure 1), we prepared stainless-steel substrates covered with a protective tape; these were partially clipped to achieve rectangle-shaped patterns. The position and shape of the rectangles on the substrate used for the fabrication of the p-type film correspond to a mirror image of those used for the fabrication of the n-type film. The n- and p-type films were electrodeposited inside the rectangle-shaped patterns with a thickness of 3.1 and $4.1 \mu\text{m}$, respectively. The electrodeposition conditions employed for the fabrication of the n- and p-type thin films were the same as those presented in Section 2. After removing the protection tapes from the substrates, only the rectangle-shaped n- and p-type films were left on each stainless-steel substrate. The n- and p-types rectangle-shaped films were then transferred onto a thin epoxy resin

(CA-147, Cemedine Co., Ltd., Tokyo, Japan) partially pasted on polyimide film (Kapton[®] film 500V, Du Pont-Toray Co., Ltd., Tokyo, Japan). After the transfer process, thermal annealing was performed under the same conditions as those described in Section 2. Next, silver pastes were painted on both ends of the n- and p-type rectangle-shaped films. The n- and p-type films were connected together, followed by drying the silver paste in air, and wrapping with thermoplastic sheets (Laminating Film, Jointex, Tokyo, Japan). The thermoplastic sheets were heat-sealed using a laminating machine.

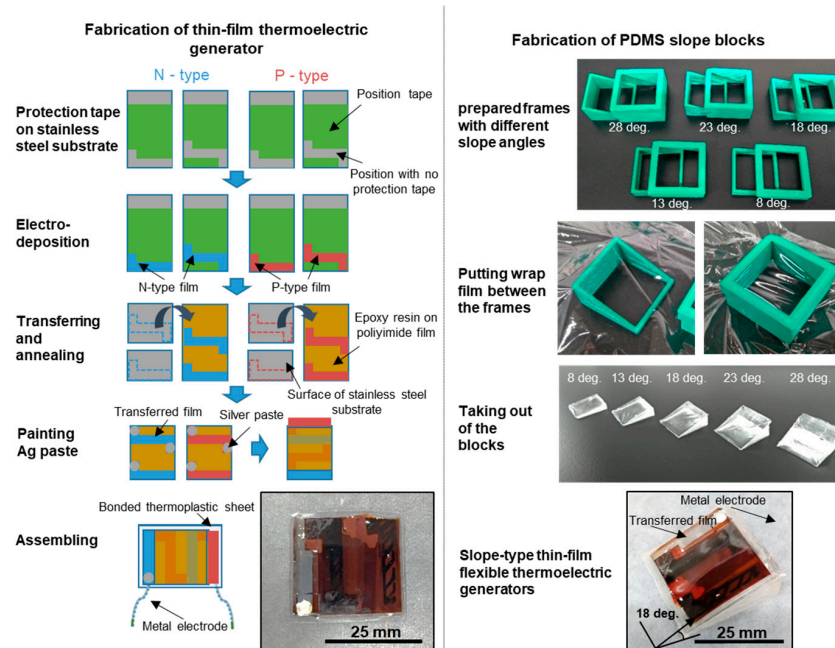


Figure 1. Schematic process flow diagram of the fabrication of slope-type thermoelectric generators.

For fabricating the PDMS slope blocks (right side in Figure 1), we first prepared frames with different slope angles (8° , 13° , 18° , 23° , and 28°) using a 3D printer (da Vinci1.0 AIO 3D, XYZ printing, Tokyo, Japan). After putting a wrap film in the frame, the PDMS (KER-4690, Shin-Etsu Chemical Co., Ltd., Tokyo, Japan) was poured into the frames, and hardened under the UV light (FL20SSBR/18, NEC, Tokyo, Japan). We put the thin-film thermoelectric generator to a PDMS slope block. Note that the generator is detachable from the slope blocks, so the same generator can be assembled with five types of slope blocks with different slope angles.

Figure 2 shows photographs of the typical slope-type thin-film thermoelectric generators with different slope angles. Each generator was commonly composed of two pairs of n- and p-type films with a length of 25 mm and width of 6 mm; the maximum heights were 6 mm (Figure 2a), 8 mm (Figure 2b), or 14 mm (Figure 2c), depending on the angle. In the all types of generator, Cu wires as electrodes were connected to the edges of n- and p-type thin films.

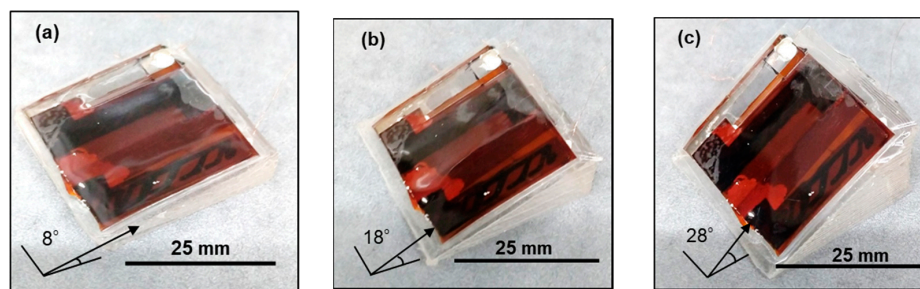


Figure 2. Photographs of typical slope-type thin-film thermoelectric generators with slope angles of (a) 8° , (b) 18° , and (c) 28° .

3.3. Performance of Thin-Film Thermoelectric Generators

We initially measured the total resistance (R_{total}), contact resistance (R_{cont}), and film resistance (R_{film}) of the thin-film thermoelectric generator, as listed in Table 2. The generator exhibited an R_{total} of 700 Ω . The resistance of two pairs of n- and p-type films (R_{film}) was estimated to be 580 Ω based on the results in Table 1. R_{cont} was calculated to be 120 Ω from the difference of R_{total} and R_{film} . The R_{cont} exhibited a relatively low value compared to our previous report [36], because the junctions between n- and p-type films in the generator were tightly connected using the silver paste.

Table 2. Total, contact, and film electrical resistances of the thin-film thermoelectric generator.

Resistances	R_{total} (Ω)	R_{cont} (Ω)	R_{film} (Ω)
Generator	700	120	580

To measure the performance of the slope-type thin-film thermoelectric generators, a temperature difference (ΔT) was applied between the ends of the generators by the simple contact of a heat source. A schematic diagram and photograph of the V_{oc} measurement method are shown in Figure 3. The temperatures on both the sides were monitored using a thermocouple (K-type) attached to the generator while the temperature of the heat source was increased. We limited the ΔT to a maximum of 15 K. When a ΔT was generated, the open circuit voltage (V_{oc}) was measured using a digital multi-meter (TR6841, TakedaRiken, Tokyo, Japan).

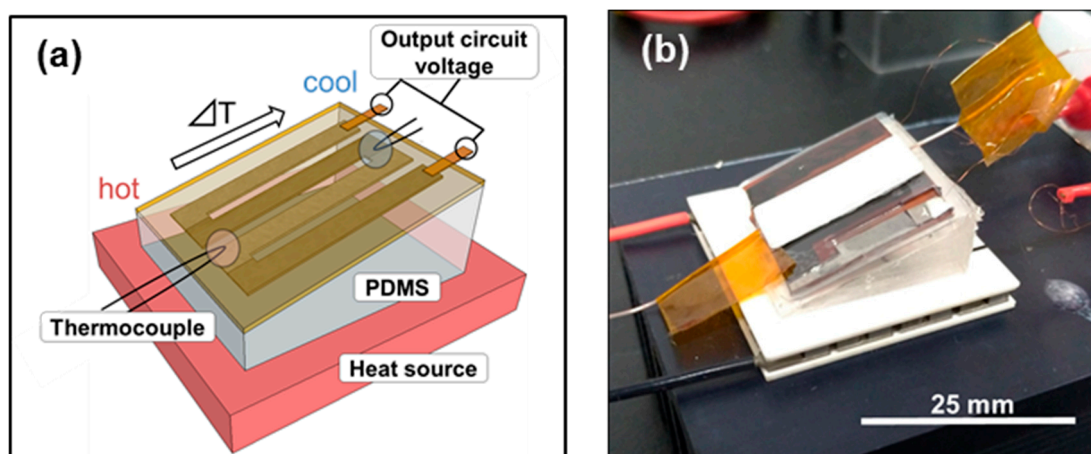


Figure 3. (a) Schematic diagram and (b) photograph of the V_{oc} measurement method.

The relationship between the temperature of the heat source and the ΔT in the slope-type thin-film thermoelectric generators is shown in Figure 4. In generators with all slope angles, the ΔT increased as the temperature of heat source was increased. For the same heat source temperature, the magnitude of ΔT became larger as the slope angle of the generator increased. This indicates that thermal conduction from the heat source to the generator was more difficult at the lower end, because of the lower thermal conduction in the PDMS slope block. The generator with the lowest angle (8°) did not reach the target ΔT of 15 K, even if the heat source temperature was increased to 47°C . However, the generator with the highest slope (28°) exhibited a ΔT of 15 K at a heat source temperature of 42°C . Therefore, we successfully demonstrated that the structure of a generator can yield sufficient ΔT by the simple contact of a heat source at around room temperature.

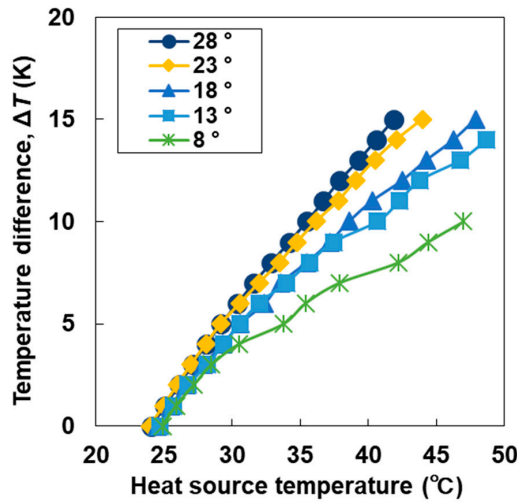


Figure 4. Temperature difference (ΔT) of slope-type thin-film thermoelectric generators as a function of the heat source temperature.

Figure 5 shows the V_{oc} of the slope-type thin-film thermoelectric generators as a function of heat source temperature and ΔT . For generators with all slope angles, V_{oc} increased as the temperature of the heat source was increased (Figure 5a). The generator with the greatest angle (28°) exhibited a V_{oc} of 7.2 mV at a heat source temperature 42°C . At the same heat source temperature, the magnitude of V_{oc} became higher as the slope angle was increased, because generators with higher slope angles obtain larger ΔT between the ends of the generator. For instance, the V_{oc} of generators at the same heat source temperature (42°C) differed by 3.2 mV for those with the highest and lowest slope angles. As shown in Figure 5b, the change in V_{oc} as a function of ΔT was the same for all slope angles, showing that V_{oc} depends on ΔT . The V_{oc} linearly increased as the ΔT increased. At the maximum ΔT (15 K), the V_{oc} of generators exhibited 7.2 mV, which almost agrees with the multiplied values among the Seebeck coefficients presented in Table 1, number of pairs and ΔT . As the thin-film generator was common to all angles of slope block, the generator was shown to have a high repetitive performance against thermal load.

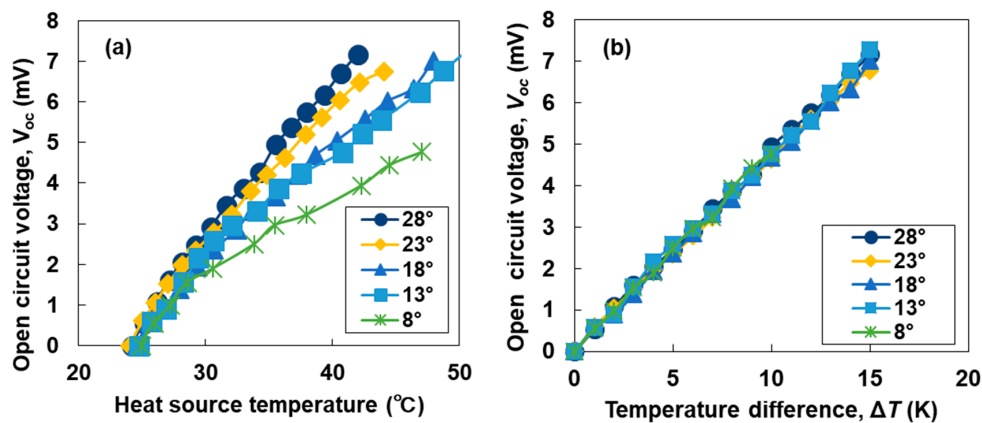


Figure 5. (a) Open circuit voltage (V_{oc}) of slope-type thin-film thermoelectric generators as a function of heat source temperature and the (b) V_{oc} of the generators as a function of temperature difference (ΔT).

Figure 6 shows P_{max} of the slope-type thin-film thermoelectric generators as functions of heat source temperature and ΔT . P_{max} is expressed as $P_{max} = V_{oc}^2 / (4R_{total})$, and the accuracy of measurement was approximately $\pm 10\%$. In generators of all slope angles, P_{max} increased as the temperature of heat source increased (Figure 6a). At the same temperature of heat source, the magnitude of P_{max} became higher as the slope angle increased. For instance, when the heat

source temperature reached 42 °C, generators with slope angles of 8°, 13°, 23° and 28° exhibited P_{\max} values of 5.5, 9.7, 11.0, and 18.3 nW, respectively. As shown in Figure 6b, the variation in P_{\max} as a function of ΔT was the same for all slope angles. This shows that P_{\max} depends on ΔT . P_{\max} quadratically increased as ΔT increased. At the maximum ΔT of 15 K, the P_{\max} of generators was 18.3 nW. The resulting P_{\max} was significantly higher than of the thin-film thermoelectric generators fabricated in our previous study [36]; this is because the thermoelectric properties of both types of thin films were increased, while the contact resistance was drastically decreased. The electric power produced in this study was sufficient to activate autonomous sensors; for example, a CMOS image sensor has a power consumption of 226 nW [44]. The generators can be employed by controlling the slope angle of the PDMS blocks according to the size of the setting space and the required amount of electric power for the target sensor.

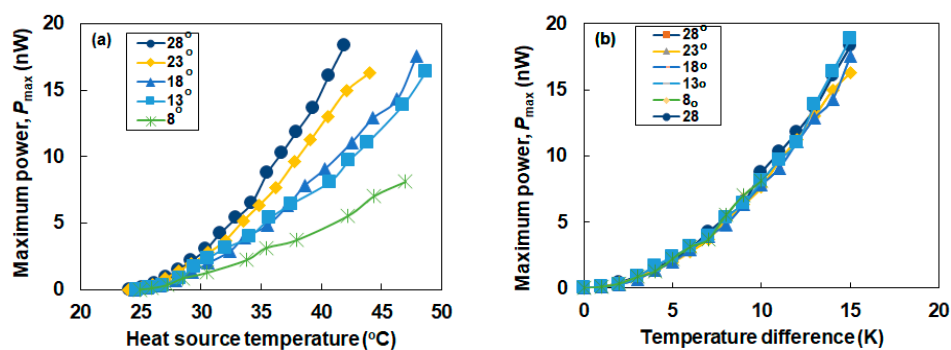


Figure 6. (a) Maximum power (P_{\max}) of thin-film thermoelectric generators as a function of temperature difference (ΔT) and (b) P_{\max} of the generators as a function of ΔT .

4. Conclusions

We fabricated slope-type thin-film thermoelectric generators with different slope angles; the generators consisted of n-type Bi_2Te_3 films and p-type Sb_2Te_3 films, and were fabricated using a combination of electrodeposition transfer, and slope block processes. Electrodeposition was performed on a stainless-steel substrate using potentiostatic electrodeposition with nitric acid-based baths. For PDMS slope blocks, frames of different angles (8°, 13°, 18°, 23° and 28°) were fabricated by a 3D printer. After placing a wrap film between the frames, PDMS was poured into the frames, and hardened under UV light. V_{oc} and P_{\max} were measured by applying a temperature difference between the ends of the generator. The generators created the temperature differences by the simple contact of a heat source. The generator with the largest slope angle (28°) exhibited V_{oc} of 7.2 mV and P_{\max} of 18.3 nW at a heat source temperature of 42 °C ($T = 15$ K). Our results demonstrate the feasibility of slope-type thin-film thermoelectric generators for low power consumption sensors, and suggest the potential benefits of fabricating the generators at a low manufacturing cost.

Author Contributions: H.Y. and M.T. conceived and designed the experiments; H.Y. performed the experiments; H.Y. analyzed the data; H.Y. contributed reagents/materials/analysis tools; H.Y. and M.T. wrote the paper.

Funding: This research was funded by JSPS KAKENHI (Grant No. 16K06752).

Acknowledgments: The authors wish to thank A. Kawahira and K. Kobiki at Tokai University for experimental support.

Conflicts of Interest: The authors declare no conflict of interest.

References

1. Hsiao, Y.Y.; Chang, W.C.; Chen, S.L. A mathematic model of thermoelectric module with applications on waste heat recovery from automobile engine. *Energy* **2010**, *35*, 1447–1454. [[CrossRef](#)]
2. Wang, Y.; Dai, C.; Wang, S. Theoretical analysis of a thermoelectric generator using exhaust gas of vehicles as heat source. *Appl. Energy* **2013**, *112*, 1171–1180. [[CrossRef](#)]

3. Kristiansen, N.R.; Snyder, G.J.; Nielsen, H.K.; Rosendahl, L. Waste heat recovery from a marine waste incinerator using a thermoelectric generator. *J. Electron. Mater.* **2012**, *41*, 1024–1029. [[CrossRef](#)]
4. Wan, Q.; Teh, Y.K.; Gao, Y.; Mok, P.K. Analysis and design of a thermoelectric energy harvesting system with reconfigurable array of thermoelectric generators for IoT applications. *IEEE Trans. Circuits Syst. I Regul. Pap.* **2017**, *64*, 2346–2358. [[CrossRef](#)]
5. Sohraby, K.; Minoli, D.; Znati, T. *Wireless Sensor Networks: Technology, Protocols, and Applications*; John Wiley & Sons: Hoboken, NJ, USA, 2007; pp. 38–58.
6. Paul, B.; Lu, J.; Eklund, P. Nanostructural tailoring to induce flexibility in thermoelectric $\text{Ca}_3\text{Co}_4\text{O}_9$ thin films. *ACS Appl. Mater. Interfaces* **2017**, *9*, 25308–25316. [[CrossRef](#)] [[PubMed](#)]
7. Paul, B.; Björk, E.M.; Kumar, A.; Lu, J.; Eklund, P. Nanoporous $\text{Ca}_3\text{Co}_4\text{O}_9$ thin films for transferable thermoelectrics. *ACS Appl. Energy Mater.* **2018**, *1*, 2261–2268. [[CrossRef](#)] [[PubMed](#)]
8. Zhao, D.; Zuo, M.; Geng, H. Enhanced thermoelectric performance of Ga-added $\text{Bi}_{0.5}\text{Sb}_{1.5}\text{Te}_3$ films by flash evaporation. *Intermetallics* **2012**, *31*, 321–324. [[CrossRef](#)]
9. Takashiri, M.; Tanaka, S.; Miyazaki, K. Determination of the origin of crystal orientation for nanocrystalline bismuth telluride-based thin films prepared by use of the flash evaporation method. *J. Electron. Mater.* **2014**, *43*, 1881–1889. [[CrossRef](#)]
10. Takashiri, M.; Imai, K.; Uyama, M.; Hagino, H.; Tanaka, S.; Miyazaki, K.; Nishi, Y. Comparison of crystal growth and thermoelectric properties of n-type Bi–Se–Te and p-type Bi–Sb–Te nanocrystalline thin films: Effects of homogeneous irradiation with an electron beam. *J. Appl. Phys.* **2014**, *115*, 214311. [[CrossRef](#)]
11. Böttner, H.; Nurnus, J.; Gavrikov, A.; Kühner, G.; Jäggle, M.; Kunzel, C.; Eberhard, D.; Plescher, G.; Schubert, A.; Schlereth, K.H. New thermoelectric components using microsystem technologies. *J. Microelectromech. Syst.* **2004**, *13*, 414–420. [[CrossRef](#)]
12. Kusagaya, K.; Takashiri, M. Investigation of the effects of compressive and tensile strain on n-type bismuth telluride and p-type antimony telluride nanocrystalline thin films for use in flexible thermoelectric generators. *J. Alloy. Compd.* **2015**, *653*, 480–485. [[CrossRef](#)]
13. Kusagaya, K.; Hagino, H.; Tanaka, S.; Miyazaki, K.; Takashiri, M. Structural and thermoelectric properties of nanocrystalline bismuth telluride thin films under compressive and tensile strain. *J. Electron. Mater.* **2015**, *44*, 1632–1636. [[CrossRef](#)]
14. Snyder, G.J.; Lim, J.R.; Huang, C.; Fleurial, J. Thermoelectric microdevice fabricated by a MEMS-like electrochemical process. *Nat. Mater.* **2003**, *2*, 528–531. [[CrossRef](#)] [[PubMed](#)]
15. Matsuoka, K.; Okuhata, M.; Takashiri, M. Dual-bath electrodeposition of n-type Bi–Te/Bi–Se multilayer thin films. *J. Alloy. Compd.* **2015**, *649*, 721–725. [[CrossRef](#)]
16. Xiao, F.; Hangarter, C.; Yoo, B.; Rheem, Y.; Lee, K.H.; Myung, N.V. Recent progress in electrodeposition of thermoelectric thin films and nanostructures. *Electrochim. Acta* **2008**, *53*, 8103–8117. [[CrossRef](#)]
17. Venkatasubramanian, R.; Siivola, E.; Colpitts, T.; O’Quinn, B. Thin-film thermoelectric devices with high room-temperature figures of merit. *Nature* **2001**, *413*, 597–602. [[CrossRef](#)]
18. Harman, T.C.; Taylor, P.J.; Walsh, M.P.; LaForge, B.E. Quantum dot superlattice thermoelectric materials and devices. *Science* **2002**, *297*, 2229–2232. [[CrossRef](#)]
19. Zhang, Y.; Chen, Y.; Gong, C.; Yang, J.; Qian, R.; Wang, Y. Optimization of superlattice thermoelectric materials and microcoolers. *J. Microelectromech. Syst.* **2007**, *16*, 1113–1119. [[CrossRef](#)]
20. Poudel, B.; Hao, Q.; Ma, Y.; Lan, Y.; Minnich, A.; Yu, B.; Yan, X.; Wang, D.; Muto, A.; Vashaee, D.; et al. High-thermoelectric performance of nanostructured bismuth antimony telluride bulk alloys. *Science* **2008**, *320*, 634–638. [[CrossRef](#)]
21. Yamauchi, K.; Takashiri, M. Highly oriented crystal growth of nanocrystalline bismuth telluride thin films with anisotropic thermoelectric properties using two-step treatment. *J. Alloy. Compd.* **2017**, *698*, 977–983. [[CrossRef](#)]
22. Kudo, S.; Hagino, H.; Tanaka, S.; Miyazaki, K.; Takashiri, M. Determining the thermal conductivities of nanocrystalline bismuth telluride thin films using the differential 3ω method while accounting for thermal contact resistance. *J. Electron. Mater.* **2015**, *44*, 2021–2025. [[CrossRef](#)]
23. Lee, J.; Galli, G.A.; Grossman, J.C. Nanoporous Si as an efficient thermoelectric material. *Nano Lett.* **2008**, *8*, 3750–3754. [[CrossRef](#)]
24. Kashiwagi, M.; Hirata, S.; Harada, K.; Zheng, Y.; Miyazaki, K.; Yahiro, M.; Adachi, C. Enhanced figure of merit of a porous thin film of bismuth antimony telluride. *Appl. Phys. Lett.* **2011**, *98*, 023114. [[CrossRef](#)]

25. Takashiri, M.; Tanaka, S.; Hagino, H.; Miyazaki, K. Combined effect of nanoscale grain size and porosity on lattice thermal conductivity of bismuth-telluride-based bulk alloys. *J. Appl. Phys.* **2012**, *112*, 084315. [[CrossRef](#)]
26. Biswas, K.; He, J.; Zhang, Q.; Wang, G.; Uher, C.; Dravid, V.P.; Kanatzidis, M.G. Strained endotaxial nanostructures with high thermoelectric figure of merit. *Nat. Chem.* **2011**, *3*, 160–166. [[CrossRef](#)] [[PubMed](#)]
27. Inamoto, T.; Takashiri, M. Experimental and first-principles study of the electronic transport properties of strained Bi₂Te₃ thin films on a flexible substrate. *J. Appl. Phys.* **2016**, *120*, 125105. [[CrossRef](#)]
28. Inamoto, T.; Morikawa, S.; Takashiri, M. Combined infrared spectroscopy and first-principles calculation analysis of electronic transport properties in nanocrystalline Bi₂Te₃ thin films with controlled strain. *J. Alloy. Compd.* **2017**, *702*, 229–235. [[CrossRef](#)]
29. Strasser, M.; Aigner, R.; Franosch, M.; Wachutka, G. Miniaturized thermoelectric generators based on poly-Si and poly-SiGe surface micromachining. *Sens. Actuators A Phys.* **2002**, *97–98*, 535–542. [[CrossRef](#)]
30. Takashiri, M.; Shirakawa, T.; Miyazaki, K.; Tsukamoto, H. Fabrication and characterization of bismuth-telluride-based alloy thin film thermoelectric generators by a flash evaporation method. *Sens. Actuators A Phys.* **2007**, *138*, 329–334. [[CrossRef](#)]
31. Hamada, J.; Yamamoto, K.; Takashiri, M. Fabrication and characterization of roll-type thin-film thermoelectric generators. *J. Phys. Conf. Ser.* **2018**, *1052*, 012129. [[CrossRef](#)]
32. Kato, K.; Hatasako, Y.; Kashiwagi, M.; Hagino, H.; Adach, C.; Miyazaki, K. Fabrication of a flexible bismuth telluride power generation module using microporous polyimide films as substrates. *J. Electron. Mater.* **2014**, *431*, 1733–1739. [[CrossRef](#)]
33. Mizoshiri, M.; Mikami, M.; Ozaki, K. P-Type Sb₂Te₃ and n-Type Bi₂Te₃ films for thermoelectric modules deposited by thermally assisted sputtering method. *Jpn. J. Appl. Phys.* **2013**, *52*, 06GL07. [[CrossRef](#)]
34. Jacquot, A.; Chen, G.; Scherrer, H.; Dauscher, A.; Lenoir, B. Modeling of on-membrane thermoelectric power supplies. *Sens. Actuators A Phys.* **2004**, *116*, 501–508. [[CrossRef](#)]
35. Takayama, K.; Takashiri, M. Multi-layered-stack thermoelectric generators using p-type Sb₂Te₃ and n-type Bi₂Te₃ thin films by radio-frequency magnetron sputtering. *Vacuum* **2017**, *144*, 164–171. [[CrossRef](#)]
36. Yamamuro, H.; Hatsuta, N.; Wachi, M.; Takei, Y.; Takashiri, M. Combination of electrodeposition and transfer processes for flexible thin-film thermoelectric generators. *Coatings* **2018**, *8*, 22. [[CrossRef](#)]
37. Scherrer, H.; Scherrer, S. Thermoelectric materials. In *CRC Handbook of Thermoelectrics*; Rowe, D.M., Ed.; CRC Press: New York, NY, USA, 1995; pp. 211–237.
38. Goldsmid, H. Bismuth telluride and its alloys as materials for thermoelectric generation. *Materials* **2014**, *7*, 2577–2592. [[CrossRef](#)]
39. Matsuoka, K.; Okuhata, M.; Hatsuta, N.; Takashiri, M. Effect of composition on the properties of bismuth telluride thin films produced by galvanostatic electrodeposition. *Trans. Mater. Res. Soc. Jpn.* **2015**, *40*, 383–387. [[CrossRef](#)]
40. Okuhata, M.; Takemori, D.; Takashiri, M. Effect of pulse frequency on structural and thermoelectric properties of bismuth telluride thin films by electrodeposition. *ECS Trans.* **2017**, *75*, 133–141. [[CrossRef](#)]
41. Takemori, D.; Okuhata, M.; Takashiri, M. Thermoelectric properties of electrodeposited bismuth telluride thin films by thermal annealing and homogeneous electron beam irradiation. *ECS Trans.* **2017**, *75*, 123–131. [[CrossRef](#)]
42. Boulanger, C. Thermoelectric material electroplating: A historical review. *J. Electron. Mater.* **2010**, *39*, 1818–1827. [[CrossRef](#)]
43. Han, Z.; Fina, A. Thermal conductivity of carbon nanotubes and their polymer nanocomposites: A review. *Prog. Polym. Sci.* **2011**, *36*, 914–944. [[CrossRef](#)]
44. Hanson, S.; Foo, Z.; Blaauw, D.; Sylvester, D. A 0.5 V sub-microwatt CMOS image sensor with pulse-width modulation read-out. *IEEE J. Solid State Circuits* **2010**, *45*, 759–767. [[CrossRef](#)]

